Surface Plasmon Resonance Bioanalytical Platform to Appraise the Interaction Between Antimicrobial Peptides and Lipid Membranes

Mihaela Gheorghiu, Sorin David, Andreea Olaru, Cristina Polonschii, and Eugen Gheorghiu

Abstract Surface Plasmon Resonance (SPR) sensors gain a wide applicability as a direct, label-free, and real-time approach to analyze biomolecular reactions occurring in the vicinity of a functionalized sensor surface. Lipid-modified sensor chips provide an accessible platform for SPR exploration of membrane—peptide interactions. While pore formation and subsequent membrane destabilization is a common feature for the interaction process between a large number of compounds such as peptides, toxins, and viruses with lipid membranes, this process has been just recently related to sensing applications.

Using POPC and melittin as model systems we show that SPR quantitative appraisal of the interaction between an antimicrobial peptide and lipid-modified sensors is capable to provide both novel sensing avenues and detailed mechanistic insights into effects of pore-forming compounds.

This new and exciting biosensing avenue is based on assessment of the nonmonotonous, concentration-dependent effect of pore formation and enables quantitative evaluation of the whole process, including full dissolution of the lipid.

Insight will be provided on a novel kinetic model that relates, via the Transfer Matrix, surface plasmon resonance (SPR) data with actual concentrations of interacting partners. In agreement with literature data, association and dissociation rates, concentration thresholds, evolution within each interacting layer of lipid and peptide concentrations, as well as of peptide to lipid ratios are derived. Although based on Biacore 3000 data, the general principles and guidelines may be applicable to other SPR assays. This biosensing approach is suitable to an entire set of pore-forming compounds including antimicrobial peptides and toxins and different lipid matrices. Recent developments in terms of surface

M. Gheorghiu (✉) • S. David • A. Olaru • C. Polonschii • E. Gheorghiu
International Centre of Biodynamics, 1 B Intrarea Portocalelor, 060101 Bucharest, Romania
e-mail: mgheorghiu@biodyn.ro http://www.biodyn.ro

W. Fritzsche and J. Popp (eds.), *Optical Nano- and Microsystems for Bioanalytics*,
Springer Series on Chemical Sensors and Biosensors (2012) 10: 183–210
DOI 10.1007/978-3-642-25498-7_6,

functionalization and electro-optical integration toward a portable analytical platform are discussed.

The proposed approach combined with appropriate design of the experimental protocol adds a new depth to the classic SPR investigation of peptide–lipid interaction offering a quantitative platform for detection, improved understanding of the manifold facets of the interaction, and for supporting the controlled design of novel antimicrobial compounds.

Keywords Bio(mimetic) sensing platform • EIS • Kinetic analysis • SPR

Contents

Abbreviations

DOPC	1, 2-Dioleoyl-*sn*-glycero-3-phosphocholine
DOPG	1, 2-Dioleoyl-*sn*-glycero-3-[phospho-*rac*- (1-glycerol)]
HBM	Hybrid bilayer membrane
HEPES	4-(2-Hydroxyethyl)-1-piperazineethanesulfonic acid
P/L	Peptide to lipid ratio
POPC	1-Palmitoyl-2-oleoyl-*sn*-glycero-3-phosphocholine
SPR	Surface plasmon resonance

1 Introduction

Pore formation and subsequent membrane destabilization is a common feature for the interaction process between a large number of compounds, such as peptides, toxins and viruses, with lipid membranes [1–3].

Assessment of the complete profile of interaction between pore-forming compounds and (cellular and artificial) membranes has potential impact in disease diagnosis, toxicology, and pharmaceutical research [4–6] and represents an important, yet under-investigated issue in biosensing.

Using the advantages offered by surface plasmon resonance (SPR) technique, i.e., label-free, real-time monitoring of analyte–ligand interaction, we propose

a novel biosensing approach based on dynamic, quantitative assessment of the concentration-dependent nonmonotonous processes associated with lipid- or cell-modified SPR platform—target analyte (i.e., pore-forming compound) interaction [7, 8]. The particular cases of melittin, a natural pore-forming peptide, and Triton X 100 detergent are considered. The comprehensive SPR measurements on melittin binding to an artificial lipid membrane (POPC) using lipid-modified L1 sensor chip (Biacore) and on cellular platforms, via a combined SPR and impedance approach, are used as a dynamic framework to highlight how to (a) retrieve quantitative information on membrane processes, (b) advance a biosensing tool, and (c) cope with matrix instability.

2 Why Antimicrobial Peptides?

Antimicrobial peptides offer an attractive solution to the problem of increasing resistance of bacteria to conventional antibiotics. The formation of transmembrane pores in the target cell is suggested as a compelling mechanism for direct interaction with membranes and subsequent lysis of the pathogen cell membrane.

Despite the already documented efficient antimicrobial activity against a wide range of pathogens and viruses [9], the potential cytotoxic activity against mammalian cells [10] limits the direct use of these peptides as therapeutics.

There are continuous efforts to modify the native antimicrobial peptides or to design new peptides to achieve better specificity against microbial infections while limiting host organism cytotoxicity.

Elucidation of the complete interaction mechanism represents a key step in peptide design and in detection of new pore-forming compounds. It requires quantitative appraisal of these compounds and access to lipid platforms for quantitative assessment of the interaction kinetics.

3 SPR Lipid Membranes

Recent advances in the preparation of stable membrane-like surfaces and the commercialization of sensor chips has enabled widespread use of SPR in protein–membrane interactions. The prerequisite was the development of surfaces that mimic natural membranes. There are two main approaches for preparation of membrane-mimetic surfaces: the hybrid bilayer membrane (HBM) and immobilized membrane bilayers (tethered). Both systems provide a well-defined model membrane in which both upper and lower layers are fluid and with an additional aqueous layer between the chip and the membrane essential for the functional incorporation of transmembrane proteins—while retaining good electrical resistance, excellent stability, and fluidity in order to sufficiently represent a pseudo-natural environment. HBM are formed on a hydrophobic surface that is generated by the deposition of an alkanethiol self-assembled monolayer (SAM) on the gold surface.

Biological molecules can be easily attached to carboxymethylated chips via amino, thiol, aldehyde, or carboxyl groups. Such covalent attachment of ligands to a dextran-layered sensor chip is probably the most common in Biacore applications. Alternatively, membrane bilayers can be tethered on the gold chip by the use of thiolipids (a thiol group, linked via a hydrophilic linker to the lipid headgroup) and thio-peptides (have a flexible linker comprising a short peptide that possesses at one end a thiol group and on the other end a lipid) [11].

One of the most popular surfaces for SPR lipid platforms is Biacore's L1 sensor chip that allows capture of liposomes or even subcellular preparations. Similar to other Biacore sensor chips, it has a dextran layer attached to the surface of the gold, while specificity is given by proprietary lipophilic groups adorning the dextrane. Here, intact liposomes are stably retained after the injection [12] or spontaneously rupture forming a bilayer [13, 14]. The dispute around actual conformation is explained by the intricate role of surface charge density and electrostatic interaction (variable with experimental conditions) in formation of supported phospholipid bilayers on molecular surfaces [15].

The type of lipids used and the dimension of the liposomes influence the SPR profile upon lipid immobilization: a maximal SPR response has been reported in the range of 11,000–12,000 RU, yet if mixtures of zwitterionic and charged lipids are used, such as 1, 2-dioleoyl-*sn*-glycero-3-phosphocholine (DOPC) and 1, 2-dioleoyl-*sn*-glycero-3-[phospho-*rac*- (1-glycerol)] (DOPG), lower amounts 7,000–8,000 RU are retained [16].

A typical protocol to form lipid membranes involves: sensor surface pretreatment to activate the binding sites, formation of the lipid membrane via liposome attachment and spreading, and chip regeneration (e.g., injections of suitable detergents).

Lipid vesicles are prepared by dissolving the lipid (e.g., POPC) in chloroform followed by drying under vacuum in a rotary-evaporator for several (three) hours. The lipid film is hydrated with (HEPES) buffer, subjected to (five) sonication cycles, 30 min/cycle and the suspension is extruded 22–25 times (using the Mini-extruder—Avanti Lipids, Alabaster, USA) through 1 μm pore membrane (polycarbonate). Stock solution (1.5 mM) aliquots are stored at +4°C prior to use.

Two–three brief washes with 100 mM NaOH are then used at a higher flow rate to remove loosely bound vesicles. An injection of bovine serum albumin is used finally to cover all nonspecific binding sites and to check for the quality of the lipid coverage.

This procedure yields homogeneous surfaces that are stable and can be directly used for binding studies.

4 Melittin–Lipid Interaction

Melittin, a 26-amino acid component of bee venom [17], is often employed as a pore-forming model compound in interaction studies with natural and artificial membranes [18–20]. Various methods are used for investigation: infrared spectroscopy

[21], fluorescence [22], transmission electron microscopy [10], X-ray diffraction [23], circular dichroism [24], and SPR [25, 26], while the distinct steps of the model of interaction, have been experimentally validated using different lipid membrane matrices: liposomes, supported lipid bilayers, micelles, phospholipid multilayers [19, 27].

Accordingly, the interaction is a complex, multiphase process, applicable to most pore-forming compounds, that exhibits concentration dependency with distinct thresholds [3, 25, 28, 29], through which melittin induces membrane disruption and lysis upon spontaneous binding to biological and model membranes [18], followed by reorientation [21], accumulation, insertion, and pore formation [3]. This interaction depends on the lipid composition and charge, on the hydration level and on the peptide concentration, orientation on membrane surface, and protonation state [30, 31].

5 Monitoring the Whole Process of Interaction Between Melittin and a Lipid Matrix

Assessment of peptide–lipid interactions by SPR assays has been reported before recommending the technique as a powerful tool for investigating real-time interactions between membrane-disrupting compounds and lipid matrices. It gave information on initial membrane attachment of pore-forming proteins [32–34] and membrane-interacting peptides [25, 26].The use of SPR and various lipid systems enabled differentiation between different steps in mechanism of action of membrane-active peptides [34–36]. Previous SPR studies on model membranes have used small (<0.37 μM) or extremely large (90 μM) peptide concentrations and 6–16 min injection times, emphasizing either attachment and insertion of the peptide [26, 28, 29] or membrane solubilization [2, 37–40], i.e., lipid disintegration as a function of peptide concentration.

These SPR analyses related the SPR sensorgrams (i.e., time variation of the reflectance dip position, or SPR angle) to the quantity of interest, assuming one effective layer (characterized by an effective thickness d_{eff}, and dielectric constant ε_{eff}) on top of the SPR chip. Simplified kinetic models [26, 28, 29], two-state or parallel reaction models, have been proposed based on equilibrium values of the overall SPR signal, without any reference to the dynamics of interacting partners.

In contrast, a longer (1 h) injection of melittin (1.6–3.6 μM), combined with a detailed kinetic model and a realistic fitting procedure [7, 8], relates the evolution of interacting compounds to the "evolving" layers on the chip and is able to provide the dynamic assessment of the whole process of melittin—lipid matrix interaction, including: melittin attachment, insertion, and membrane solubilization at various peptide-to-lipid ratios (P/L).

To this end, a mathematical model comprising a system of kinetic equations to describe the evolution of lipid and peptide concentrations within distinct layers on the chip as well as a procedure, based on Transfer Matrix Analysis, to relate the kinetics to the SPR has been designed. This approach is applicable to other SPR

techniques (waveguide spectroscopy [41, 42] and interferometry [20, 43]) and not only to the Biacore assay [44].

A representative SPR experiment concerning peptide–lipid interaction is presented in Fig. 1a and highlights the distinct steps involved in the assay: (a) Sensor chip pretreatment; (b) Formation of lipid matrix as a model cell membrane for investigation of the pore-forming peptide binding; (c) Removal of the loosely bound vesicles structures; (d) Peptide–lipid interaction; and (e) Sensor regeneration. Figure 1b reveals the multiphase process involved in peptide-to-lipid interaction: attachment, attachment and insertion, and lipid dissociation.

6 SPR Bioanalytical Platform

The effective thickness d_i and dielectric constant ε_i of each layer in the system shape the reflectivity spectrum, influence the SPR angle and are important parameters in the construction of a transfer matrix (see Fig. 2). The Transfer Matrix [45] involves repeated application of the Fresnel equation [46], and relates, in conjunction with a kinetic model, the SPR angle shift to the surface concentration of compounds in the multilayer system associated with the experimental platform.

The transfer matrix combines the entire set of field components and involved layers and can therefore be used to calculate the reflectivity of the complete system provided that thickness and refractive index of all layers, the wavelength, and the angle of incidence θ are given.

To derive the time evolution of the dielectric permittivity, for each layer comprising a mixture of different dielectric media, the following equivalence has been used [47]: $\varepsilon_{\text{ech}}(t) = \sum_i \Phi_i(t) \times \varepsilon_i$ where $\Phi_i(t)$ is the actual volume fraction of the compound indexed i that obeys the $\sum_i \Phi_i(t) = 1$ rule. According to Fig. 3, four distinct layers are considered: the layer above the lipid where the peptide attaches, the actual lipid layer where melittin inserts and eventually forms aqueous pores, the layer on top of L1 matrix where, upon lipid dissociation, the peptide can attach, and last, the bulk, characterized by a mixture of running buffer and peptide of various concentrations.

The equivalent dielectric permittivities for each layer have been considered within the transfer matrix to compute the variation of the position of the reflectance minimum (the SPR angle) and relate it with the SPR data. This algorithm and the proposed model have been used to fit the experimental data, to derive the concentration thresholds and kinetic parameters for each constitutive phase (association, insertion, and lipid membrane destabilization) and provide time evolutions of actual P/L ratios within each layer.

The hallmarks of this fitting routine are:

1. Numerical integration of the set of four coupled differential equations for the concentrations of each component in the multilayer system.

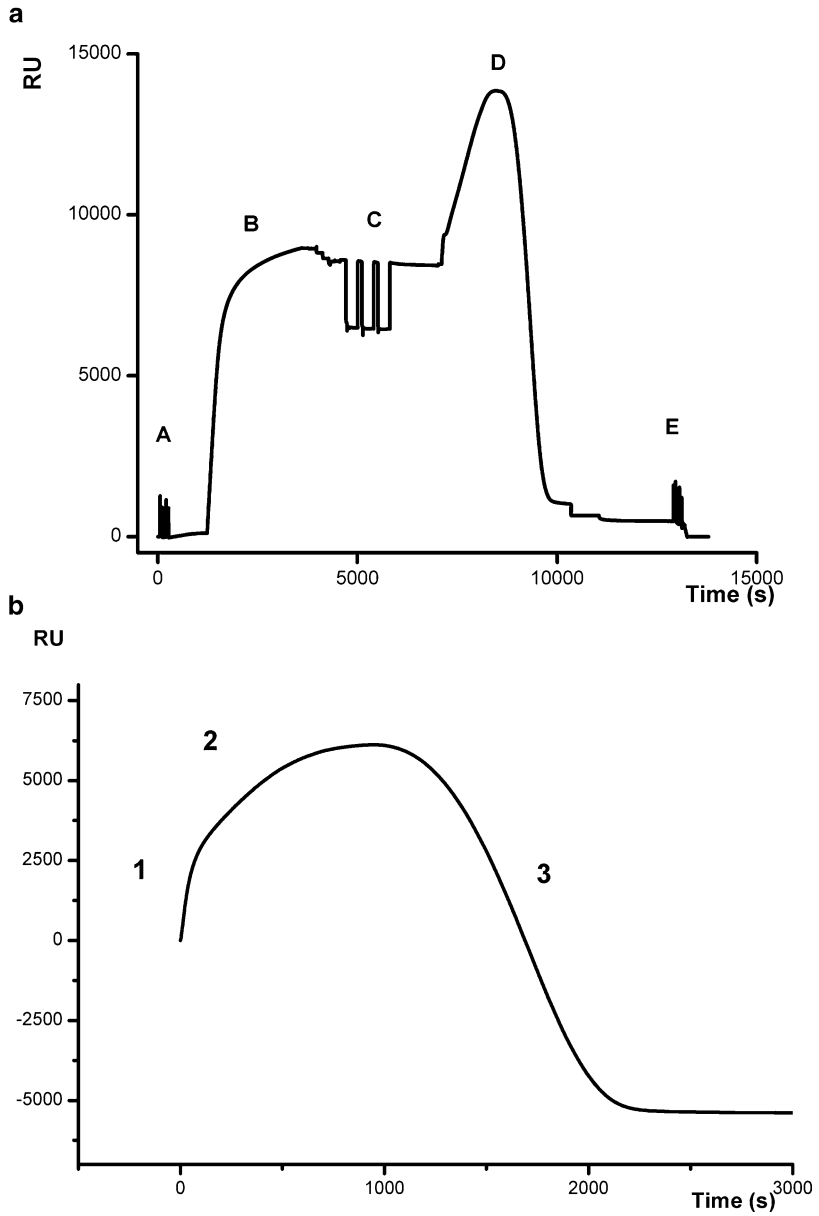

Fig. 1 (**a**) Steps of the SPR assay (A) Sensor chip pretreatment; (B) Formation of lipid matrix as a model cell membrane for investigation of the pore-forming peptide binding; (C) Removal of the loosely bound vesicles structures (D) Peptide–lipid interaction and (E) Sensor regeneration. (**b**) Representative sensorgram detailing step (D), Peptide–lipid interaction normalized to the moment of peptide injection (1) attachment, (2) attachment and insertion, (3) lipid dissociation

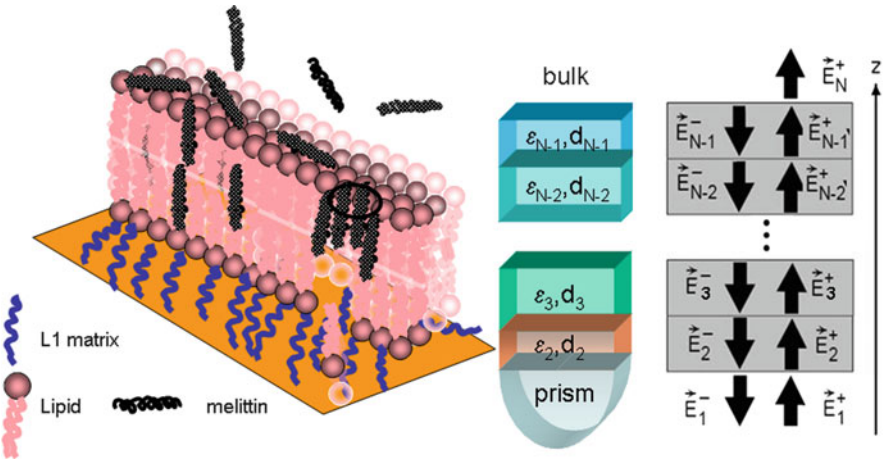

Fig. 2 The multilayer structure of the lipid platform, each component, characterized by thickness d_i and complex dielectric constant ε_i. The set of layers is considered stacked between a hemispherical prism (Biacore 3000 set-up) with dielectric constant ε_p and the semi-infinite medium (running buffer) with dielectric constant ε_h. The corresponding Transfer Matrix is constructed by considering the field distribution, reflection, and transmission within each component of the multilayer system

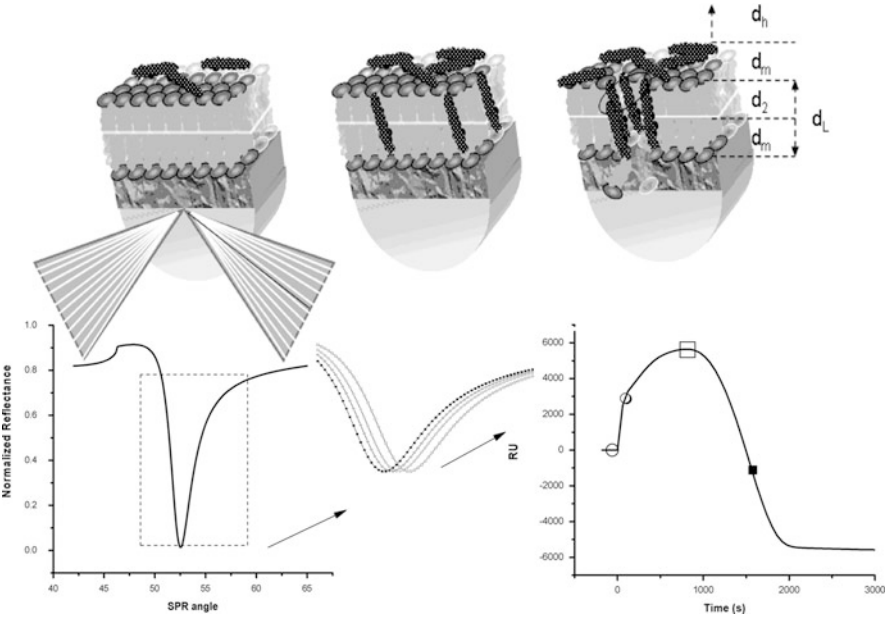

Fig. 3 Schematic representation of peptide–lipid interaction steps, the equivalent layers of the lipid platform and the corresponding SPR data (SPR angle and sensorgram)

2. Computation of the effective permittivity of the distinct layers. Relate volume concentrations to corresponding volume fractions in the distinct layers.
3. Derivation of the SPR angle based on the application of the transfer matrix on the multilayer system. As the SPR sensorgram is expressed in relative units, 8.2 Relative Units for every millidegree SPR angle shift equivalence relation has been used for Biacore 3000 data [48].

The detailed numerical analysis of SPR measurements for the kinetic characterization of the complete interaction process between melittin and lipid membranes is made under two assumptions, based on experimental findings: (1) a homogeneous planar lipid coating uniformly covers the L1 surface and (2) the interaction of the peptide with the lipid matrix is not dependent on the multi-bilayer structure of the lipid coating.

The first assumption is consistent with current knowledge (theoretical [49] and experimental [13, 15] evidences) on rupture of adsorbed (zwitterionic) lipid vesicles to form supported phospholipid bilayers when strong interaction with the substrate surface, appropriate surface charge density, appropriate buffer, and a prior large-size liposome accumulation to the surface conditions are met. Based on the second assumption, different thicknesses of the lipid matrix (not individual layers) are considered to account for different SPR signals upon lipid immobilization.

7 The Kinetic Model

The dynamics of the nonmonotonous process of interaction, as revealed by the SPR signal, is highly dependent on the balance between the kinetics of melittin association and insertion, which in turn are modulated by the surface and bulk concentrations of melittin. With increasing peptide binding, upon reaching a threshold, melittin begins to insert into the membrane and undergoes reorientation [50].

Designed in compliance with the present mechanistic knowledge, the set of kinetic equations are related to distinct steps of interaction (e.g., attachment and insertion) and provide time evolution of both lipid and melittin concentrations as function of several threshold concentrations (m_0, m_i, and m_L) and constants: K_{a1} for association, K_{a2} for melittin insertion, K_{d0} for melittin dissociation, and K_{dl0} for lipid membrane destabilization:

– Association

$$m'[t] = K_{a1}N_m(N_l[t] - m[t]) \times H[N_l[t] - m[t]] - K_{d0} \times N_l[t]/N_{l0} \times m[t] \times H\left[N_l[t]\right] - k_{ai} \times m'_{ins}[t], \quad (1)$$

where K_{a1} is the association constant, N_m is the bulk concentration of melittin, $N_l[t]$ is the number of available "binding sites" associated with the immobilized lipid,

m'_{ins} stands for kinetics of melittin insertion in the lipid matrix, and K_{d0} affects the dissociation induced by flow conditions.

– Insertion

$$m'_{\text{ins}}[t] = K_{\text{a2}}\left(m[t] - m_0\frac{N_1[t]}{N_{\text{l0}}}\right) \times \left(m_{\text{i}}\frac{N_1[t]}{N_{\text{l0}}} - m_{\text{ins}}[t]\right) \times H\left[m[t] - m_0\frac{N_1[t]}{N_{\text{l0}}}\right] \times H\left[m_i\frac{N_1[t]}{N_{\text{l0}}} - m_{\text{ins}}[t]\right], \tag{2}$$

where K_{a2} is the insertion constant, $m[t]$ is the concentration of associated melittin, m_0 is threshold for melittin reorientation and insertion into the membrane, and m_{i} is the threshold concentration that limits the progression of insertion.

– Lipid destabilization and dissociation

$$N'_1[t] = -K_{\text{dl0}}\frac{N_1[t]}{N_{\text{l0}}}\left(m[t] - m_{\text{L}}\frac{N_1[t]}{N_{l0}}\right) \times H[N_1[t]] \times H\left[m[t] - m_{\text{L}}\frac{N_1[t]}{N_{\text{l0}}}\right] \tag{3}$$

where m_{L} is the threshold concentration of associated melittin that triggers lipid destabilization, K_{dl0} is the lipid dissociation constant

– Direct melittin binding to the uncovered L1 chip, as melittin is injected as well during lipid dissociation stage,

$$m_{\text{L1}}{}'[t] = K_{\text{a3}}N_{\text{m}}(RR - N_1[t]/N_{\text{l0}}) \times (N_{\text{CO}} - m_{\text{L1}}[t]) \times H[RR - N_1[t]/N_{\text{l0}}] \times H \times [N_{\text{CO}} - m_{\text{L1}}[t]] \tag{4}$$

where K_{a3} is the related association constant, RR is the percentage of uncovered sensor and N_{C0} is the concentration of L1 binding sites for melittin.

Due to the structure of the kinetic equations (comprising terms accounting for thresholds—represented by step functions H[x]), and the inherent complexity of the SPR response of the evolving layers involved in peptide–membrane interaction, no analytical solution exists.

The set of coupled differential equations [8] provides the dynamics for each of the components within the multilayer system which are related via the transfer matrix to the SPR angle corresponding to the actual SPR data (Fig. 3). As such, the model allows a high degree of flexibility with no a priori consideration of a molecular model of interaction. It enables compact evaluation of rather diverse SPR data (e.g., different peptide concentrations on similar lipid coverage—Fig. 4a, and extreme P/L ratios—Fig. 4b), independent of the sensor characteristics. These representative data at different P/L ratios show significant variability in the measured values, dependent on the peptide concentration and lipid immobilization level. Peptide concentration influences the slopes of the upward and downward regions (attachment and insertion and lipid destabilization

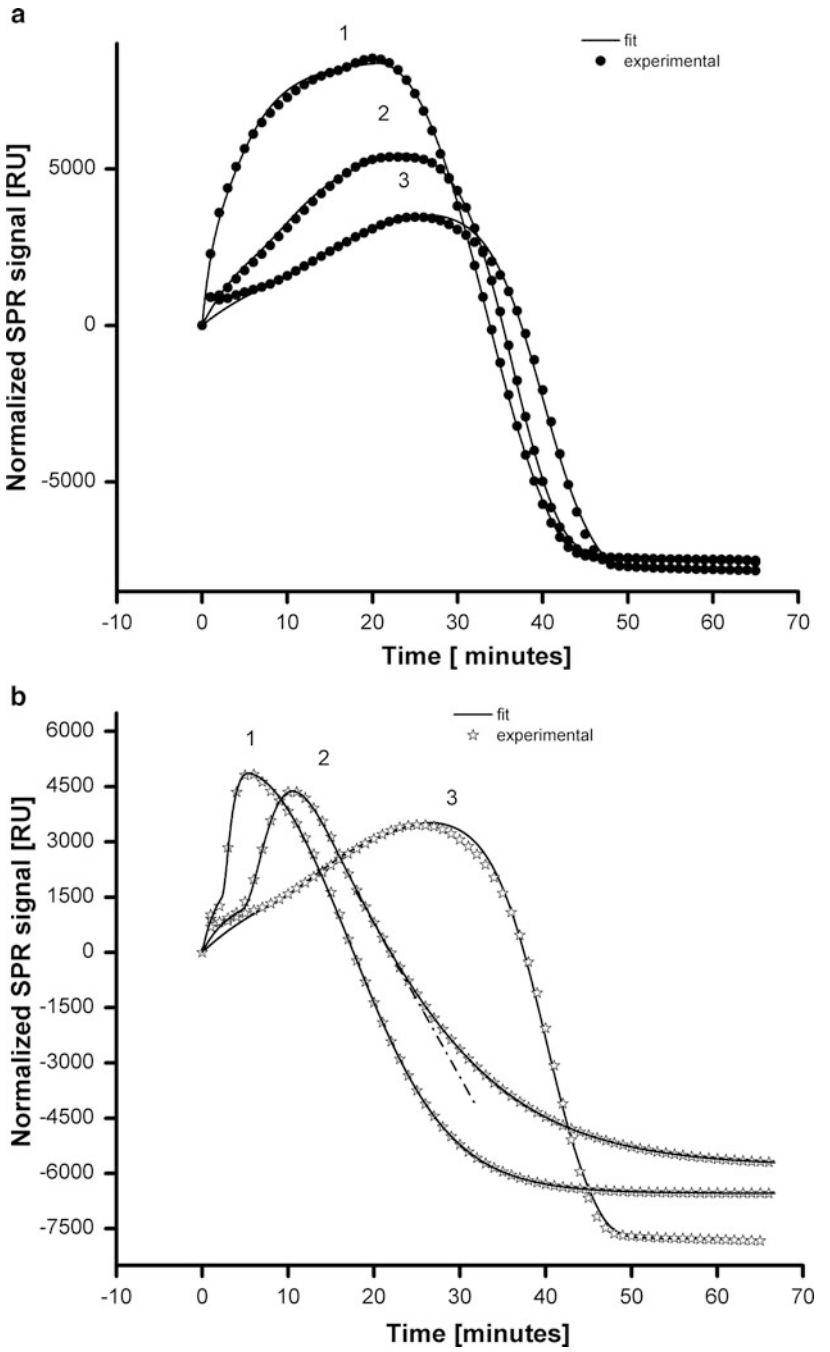

Fig. 4 (**a**) Characteristic SPR sensorgrams (experimental and fitted curves) corresponding to different melittin concentrations (1) 2.55 μM, (2) 2.43 μM, and (3) 2.35 μM, injected to similar

respectively): the higher the peptide concentration, the steepest the slope and the earlier the occurrence of the peak, while the lipid amount in conjunction with peptide concentration, modulates the level of the peak (the higher the peptide concentration and the lipid level, the higher the summit level).

8 Relevance

The proposed sensing platform has far-reaching implications:

1. Provides the pattern of evolution of the complex, nonmonotonous process of peptide–lipid interaction and a direct way to quantify the concentration of peptide.
   Fitting the experimental data (Fig. 4), the model provides kinetic parameters and time evolutions of concentrations of melittin, attached and inserted (Fig. 5), and related volume fractions of the lipid (Fig. 6), comparable with data reported in the literature.
   Despite model limitations (e.g., advancement of insertion process assessed only as the progress of the areas where full insertion of melittin has occurred, a homogenous structure of the lipid membrane), we consider that the evolution of the effective peptide attached or inserted provided by our approach is consistent with the actual overall molar values. As such, the evolution of the actual P/L ratios can be as well derived [8].
2. Enables novel biosensing avenues:
   In "classical" biosensing platforms, there is a monotonous time evolution of measured parameter(s) as a function of the target analyte, thus allowing for equilibrium analysis or use of arbitrary chosen time points to examine an interaction or for quantification.
   Since the interaction between a pore-forming compound and a lipid membrane is related to a nonmonotonous effect determined by the target analyte, a novel sensing procedure to quantify the concentration of melittin is proposed [7].
   The pattern of evolution of the complex, nonmonotonous process of peptide–lipid interaction provides a direct way to quantify the concentration of melittin. Specifically, the concentration of the test compound can be inferred from T_{max}, the time point when the nonmonotonous evolution of SPR signal due to peptide–lipid interaction reaches its summit. The timing of this characteristic value is related to the ability of the pore-forming compound to insert into and destabilize the lipid matrix. It occurs during pore formation and destabilization of lipid membrane

Fig. 4 (continued) lipid coverage ~8,550 RU lipid. (**b**) Characteristic SPR sensorgrams (experimental and fitted curves) corresponding to extreme P/L: low lipid versus high melittin concentration (1) 6,500 RU lipid—3.62 μM melittin and (2) 5,800 RU—2.81 μM melittin, high lipid versus low melittin concentration (3) 8,600 RU lipid—2.35 μM melittin

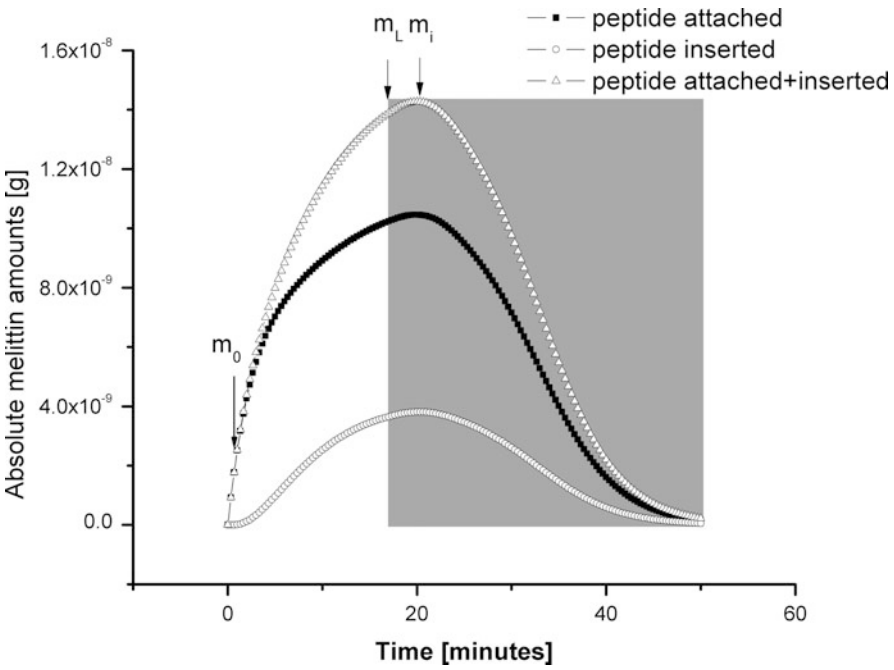

Fig. 5 Characteristic evolutions of derived absolute amounts of peptide attached and inserted on POPC lipid matrix (8,800 RU) upon ~1 h injections of melittin (2.6 μM). Also indicated are the time points when they are attained: the threshold concentrations for initiation of insertion, m_0, of lipid dissociation, m_L, and limiting peptide insertion, m_i. Lipid dissociation that affects both peptide insertion and attachment is indicated as the *gray zone*

phase due to dynamic removal of lipids (and associated peptide) from the sensor surface once a destabilization threshold of peptide is reached.

The timing of this characteristic value is related to the ability of the pore-forming compound to insert into and destabilize the lipid matrix. It occurs during pore formation and destabilization of lipid membrane phase due to dynamic removal of lipids (and associated peptide) from the sensor surface once the destabilization threshold of peptide is reached. Such a calibration curve (Fig. 7a), based on $T_{max,}$ does not require any theoretical assumption or modeling, yet for large T_{max} (corresponding to small peptide concentrations) $1/T_{max}$ is asymptotically progressing toward 0, rising experimental difficulties in determining T_{max}.

As revealed by the occurrence of T_{max}, there are two aspects that lead to a nonlinear behavior:

- Lipid dissociation occurs upon melittin accumulating and reaching sequentially two threshold concentrations: one corresponds to the beginning of insertion, and the other one to initiation of lipid destabilization.
- The larger the peptide concentration, the larger the SPR signal related to the direct peptide–lipid binding. This process is significant in the first few, up to 5 min (for the highest melittin concentration considered 3.5 μM), masking the

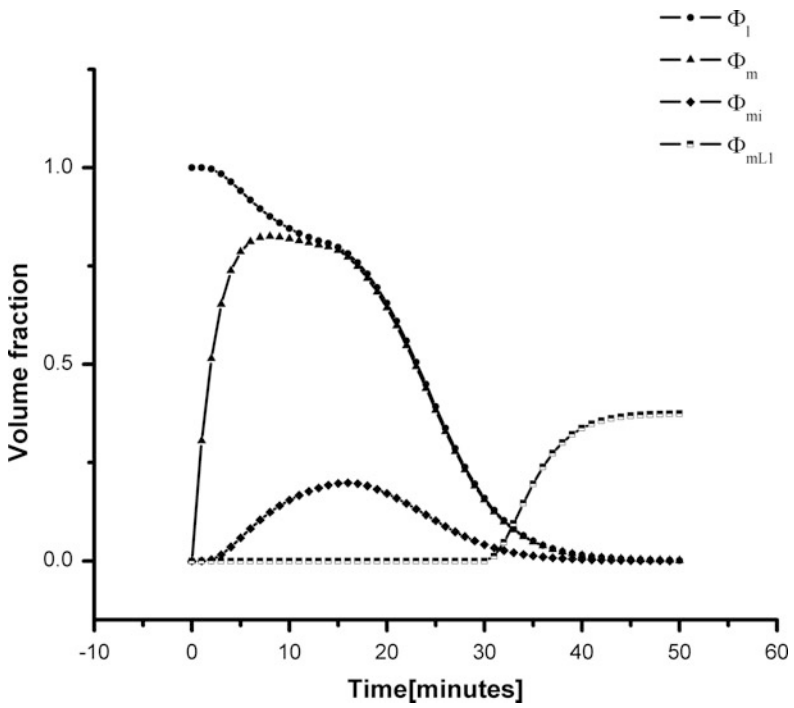

Fig. 6 Derived volume fractions of lipid, within the lipid matrix, and of melittin a) associated with the lipid Φ_m, inserted in the lipid matrix Φ_{mi} or associated directly with the L1 matrix Φ_{mL1} upon lipid destabilization and removal

decrease in the SPR signal due to lipid dissociation and correspondingly delaying the occurrence of T_{max}.

Additionally, as revealed in Fig. 7b, the proposed set of differential equations can be also used to assess T_{ins} (the moment when the peptide insertion is initiated), which proves useful in deriving the concentration of the pore-forming compound and hence supports the "biosensing process". The linearity domain is nevertheless limited since, for large peptide concentrations, the lipid dissociation and possible bulk effects can shadow the SPR signal connected to melittin attachment and insertion.

We envisage that this approach is able to support accurate detection and that the related analysis platform, could be further extended to membranes with different lipid compositions and other pore-forming compounds, as well.

3. Provides checking tools for sensing platform optimization: L1 regeneration conditions are not fully optimized [51, 52]; hence lipid coating reproducibility in time can change dramatically. Therefore, assessment of melittin attachment directly to the chip [as described by (4)] in relation to different regeneration conditions could support improvement of the experimental protocol toward sensing applications.

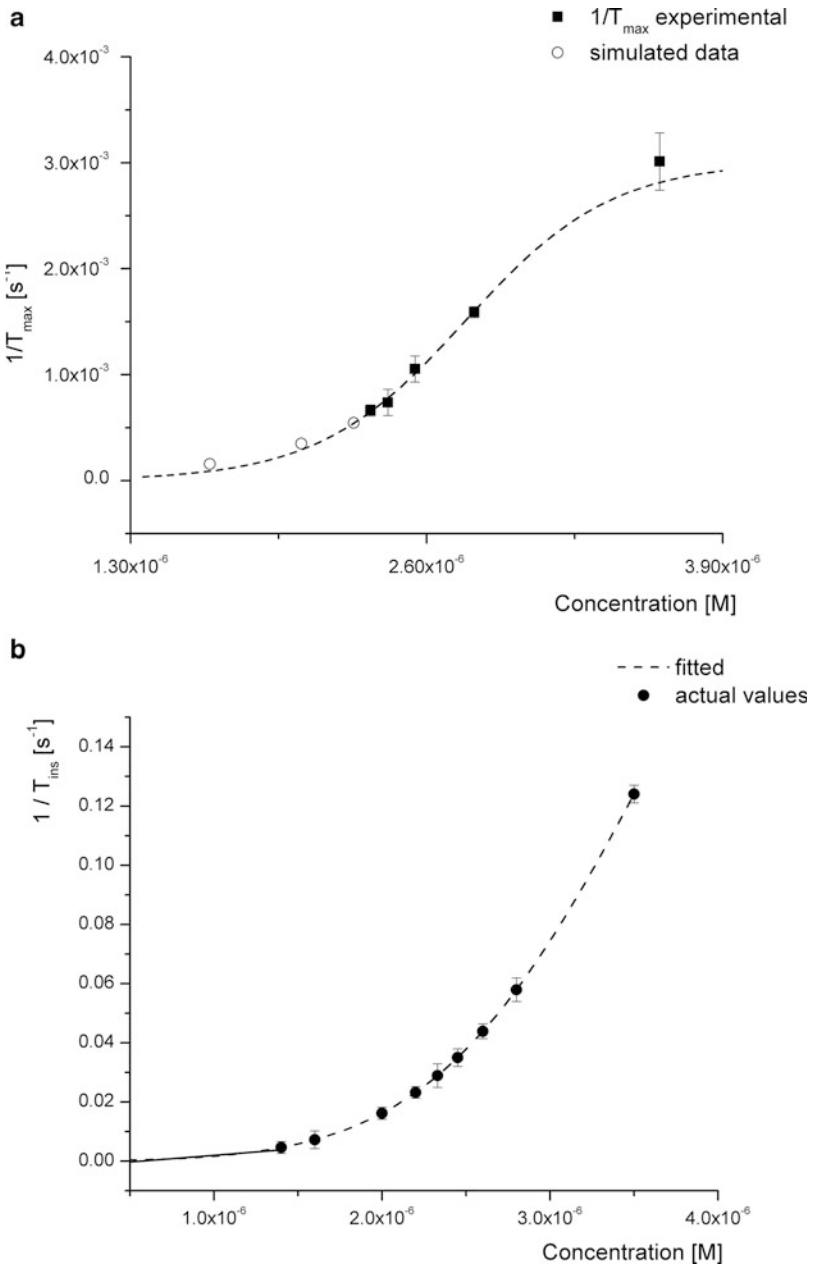

Fig. 7 (**a**) Calibration curve based on T_{max}, the time point when the nonmonotonous evolution of SPR signal due to peptide–lipid interaction reaches its summit, within the experimental data *square* and simulated *open circle* based on the model and corresponding to low peptide concentrations. (**b**) Calibration curve based on the moment when the peptide insertion is initiated (m_0 threshold according to the kinetic model)

Moreover, the same transfer matrix approach can be used in characterizing the L1 matrix and subsequently the lipid membrane attached on the surface.

4. Supports insight on interaction mechanisms depending both on various antimicrobial peptides and lipid composition of lipid membrane. We consider the L1 chip as a scaffold to analyze the process of interaction between a pore-forming compound and a lipid matrix. The composition of the lipid membrane developed on top of the L1 chip depends only on the composition of the vesicles in solution upon lipid matrix formation. Moreover, the target of antimicrobial peptides is believed to be the lipid membrane regions of bacterial and fungal biomembranes, regardless of their final cellular targets, with lipid composition (including cholesterol) playing a determinant role [53].
   As many factors (including temperature, lipid composition, pH, or presence of a synergistic partner peptide) determine how membrane-active peptides interact with the lipid bilayer, different modes of membrane interaction have been suggested: (a) binding to the bilayer or water interface; (b) "carpet"-like interaction; (c) detergent-like action; (d) disintegration of the bilayer producing bicelle-like discs; (e) transient or long-lived "barrel-stave"; (f) "toroidal" or "wormhole" pores; (g) insertion into a transmembrane alignment; (h) formation of a "slit"; (i) diffusion across the membrane; (j) modulation of the membrane curvature, induction of non-bilayer lipid phases and/or translocation via an inverted micelle [54].

Among these, most commonly considered are pore formation via a "barrel – stave" mechanism or by membrane solubilization (detergent-like) "carpet" mechanism. Both mechanisms depend on the peptide charge and the mode of self association in the target membrane [3, 55]. Nevertheless, the latter gains more and more support from experimental and molecular dynamics simulation data [56–58] as the general model of interaction of antimicrobial peptides with lipid membranes.

Though the SPR approach does not provide details on the molecular interaction mechanism, it is worth noting that our results show that lipid dissociation is largely dependent on randomly associated/inserted melittin, with no defined pore structure. This makes our results consistent with "carpet-like"/"toroidal pore" models. A further confirmation is provided by SPR analysis of specific action of a detergent (Triton X 100) on POPC lipid membranes revealing similar, nonmonotonous patterns of evolution (Fig. 8).

The proposed approach for lipid matrix formation is applicable for various lipid matrices with slight modification of the immobilization protocol. Tests have already been made for simple anionic (POPG) and mixtures of anionic and zwitterionic lipids (POPG:POPC) with 2.6 μM melittin concentration (Fig. 9).

As such, the proposed approach is a suitable experimental platform for accessible evaluation of the interaction of peptides/pore-forming compounds, capable to support detailed mechanistic research in conjunction with complementary techniques. Having in view the similar interaction patterns reported [2] for virus mimetic attack, we stress on a wider applicability of our approach for quantitative

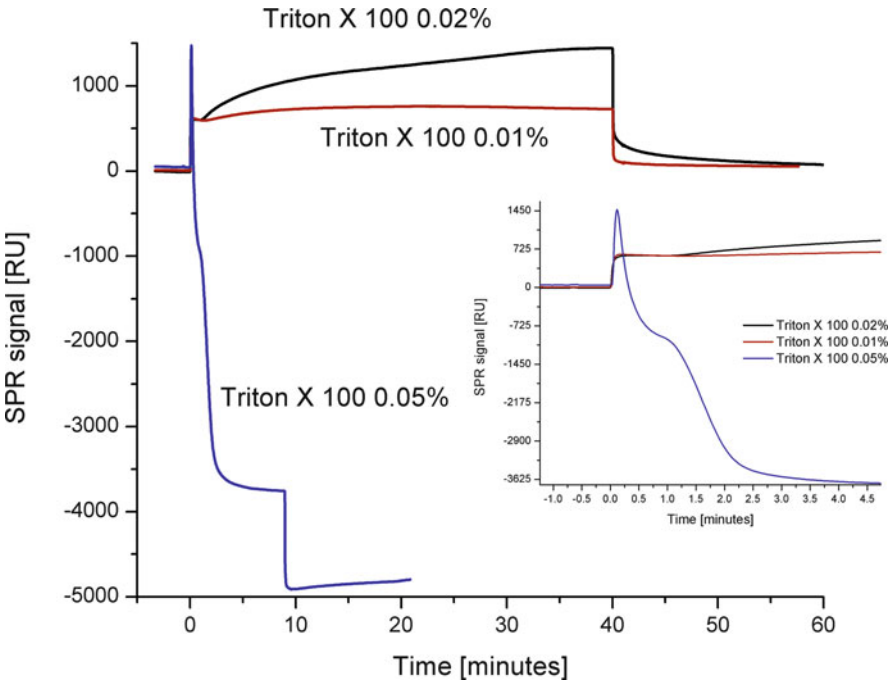

Fig. 8 Lipid detergent interaction for three concentrations of Triton X 100 a nonionic detergent. *Inset*, focus on the first 4 min after injection revealing nonmonotonous dynamics concentration dependent

assessment of the effect of other pore-forming compounds on different lipid membranes, thus on a broader biophysical significance. Nevertheless, the assessment of other systems should involve amendments of both kinetic model and Transfer Matrix approach in agreement with data concerning layer structure, molecular arrangements, etc.

9 Whole Cell Approach

While further enrichment with proteins (proteoliposomes [59]) and cholesterol (mixed liposomes [10, 60]) is possible for these synthetic membranes, the complexity and dynamics of natural cell membranes recommends the use of cellular extracts or directly the target cells.

There are inherent limitations of SPR assessment of biological cells related to: (a) the depth of the sensitivity domain (reaching down to several hundreds of nanometers) versus the actual dimensions of the cells (microns), (b) the large cell dimensions versus the fluidics of commercial instrumentation (e.g., 20 μm for

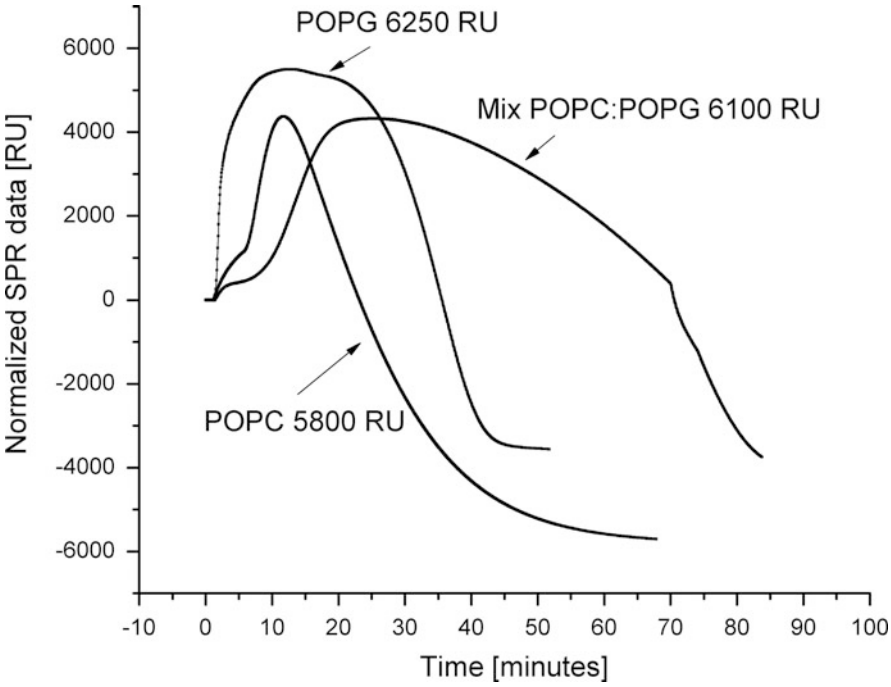

Fig. 9 Interaction of melittin with lipid matrices of different compositions: zwitterionic (POPC), anionic (POPG), and mixture (3 POPC:1 POPG); 2.6 μM melittin concentration

Biacore) rendering a high probability of flow cell clogging, (c) the surface and volume inhomogeneity related to highly variable biological cells randomly attached to the surface.

The SPR analysis using commercial instrumentation such as Biacore 3000 and the proposed kinetic model presented so far is based on the fact that all changes in adsorbed mass within the SPR sensitivity domain are revealed by the corresponding SPR value. While decomposition (seen as lipid dissociation, with subsequent removal from the surface due to continuous injection of lipid-free running buffer with peptide) is encompassed by the model, there are inherent limitations of the Biacore SPR approach (basically an "effective refractive index" method) to reveal localized, discrete processes such as the eventual deformation of a cell.

Hence, in relation to the necessary cellular assays, we propose a combined SPR and impedance approach to test for the direct effect of model pore-forming compounds on mammalian cells. This approach could bring significant advantages versus (pre)clinical trials (prone to high costs and rising ethical issues) for optimization and evaluation of the efficiency in modifying the native antimicrobial peptides or designing new peptides to achieve better specificity against microbial infections while limiting/eliminating their cytotoxic activity.

To this end, a combined SPR and impedance system based on the SPREETA TSPR2K23 SPR sensor (Texas Instruments, TX, USA) has been developed within

the International Centre of Biodynamics, Bucharest, Romania. The combination of SPR with impedance investigations is straightforward as the thin gold films used for the generation of surface plasmon waves can be simultaneously used as sensing electrodes.

Impedance evaluation has matured into a powerful technique for monitoring cellular systems. It is based on measuring the response (current and its phase) as a function of frequency of an electrochemical system to an applied weak, noninvasive oscillating potential (up to 50 mV) in the frequency range 1 Hz–10 MHz.

As proven by the commercially available ECIS type devices [61], attachment and spreading of cells on the electrode surface change the impedance in such a way that morphological information of the attached cells can be directly inferred enabling noninvasive, continuous assessment of cell attachment, spreading, and proliferation. The inherent sensitivity and ability to eliminate stray effects are dependent on the electrode geometries, measurement set-up, integration of controlled flow through capabilities, and complementary analytic methods (e.g., optical). The technique (a) can provide valuable real-time cellular activities of viable cells, (b) it is a label-free method, (c) it is more sensitive in monitoring early cell responses compared with traditional image analysis, and (d) it reveals quantitative information about the cell responses in a dose-dependent manner. Nevertheless, the appropriateness/uniqueness of the circuit model influences the quality of the parameters derived from experimental data. Both microscopic [62–64] and circuit models [65, 66] are available and can be integrated for real-time data analysis and the combination with SPR could provide some internal control conditions (Fig. 10).

The circuit elements required for accurate modeling of the impedance experimental data are presented in Fig. 11 and are related to: interfaces at the two electrodes—constant phase elements (CPE), allowing suitable parameterization of chip nonhomogeneities; R1 and R3—representing the metal layer's resistance and C3 and C4 the equivalent capacitance of the cell layer covering each electrode; R2 and C2 are the resistance and capacitance of the solution over the electrodes [66].

From the difference between the impedance of the chip with cells and the impedance of the chip without cells (in the same experimental conditions), we obtain the information on cell impedance as:

$$Z^*_{\text{cells}} = Z^*_{\text{withcells}} - Z^*_{\text{withoutcells}}. \tag{5}$$

The corresponding resistance and capacitance of cell layer is derived for each frequency and time points.

The system developed combines the label-free monitoring capabilities of both techniques for affinity detection and cell-based biosensing helping to overcome some of the limitations both techniques have when used alone.

The system schematically presented in Fig. 12 enables optical and electric addressing of interfacial processes related to a wide choice of functional surfaces and flow conditions. Polymer thin films or matching liquids (this is the convenient approach used in the following) enable optical interfacing with chips with variable configurations.

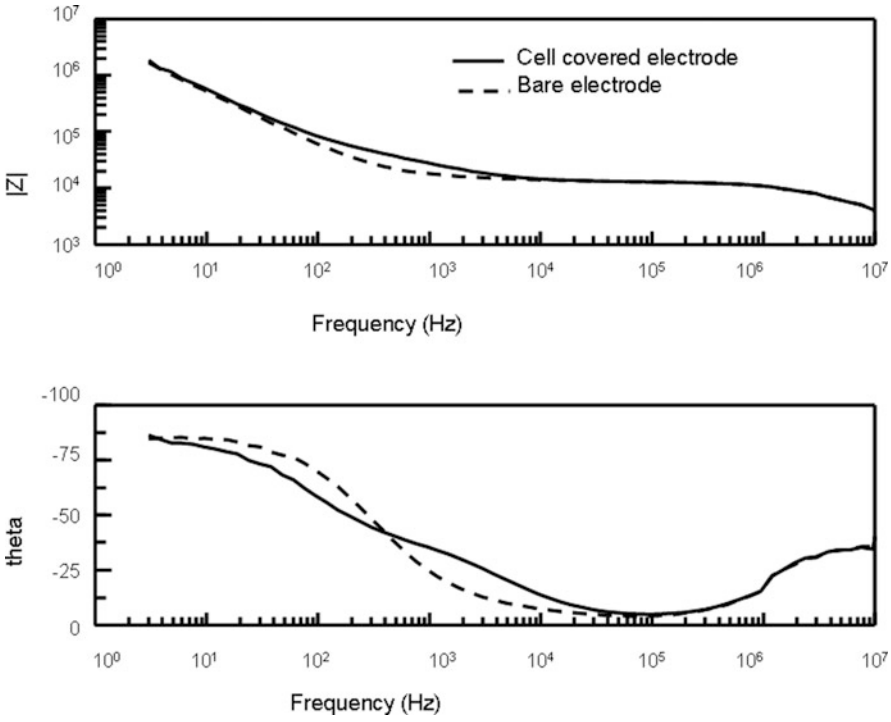

Fig. 10 Impedance spectra (magnitude and phase) of the electrodes with (*black line*) or without cell (*dashed*)

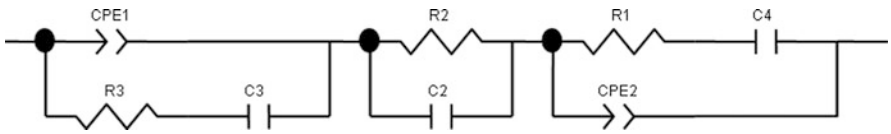

Fig. 11 Equivalent circuit—cell-coated electrodes

Polydimethylsiloxane (PDMS) flow cells are mounted on the Spreeta sensor and the liquid sample is delivered over the sensor surface by the automated fluidic system comprising syringe pumps and valves actuated by computer.

The flow rate range is 40–1,000 µl/min with increments of 1 µl/min. Sample injection is achieved using electrically actuated injection valves, one for each flow circuit. The sample loops of the injection valves are loaded with the desired sample through a selection valve and injected in the system simultaneously or independently. Sample loading, injections, and washing protocol are preprogrammed and the user has only to select the measurement flow channel, the sample volume, and flow rate of the buffer or sample. Data acquisition and processing is realized with an interface controlled by a LabView software. The signal received

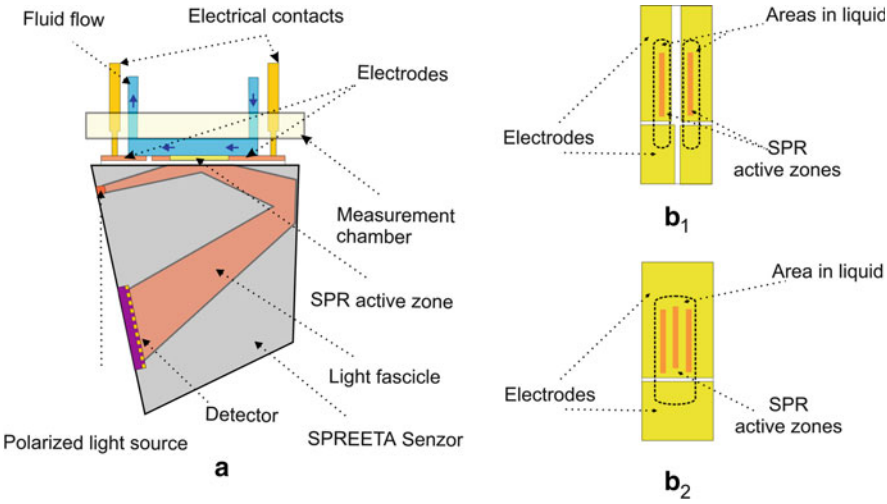

Fig. 12 Combined SPR and impedance set-up (**a**) with dual (**b1**) and living cells (**b2**) flow cells

from the SPR sensor is processed through various software routines to subtract background and reference data in order to obtain the SPR curve. The SPR minimum is calculated online by analysis of the SPR curve. This data is converted then to refractive index units, or response units using a calibration protocol. The software also allows saving the SPR data (as refractive index units or response units) as well as the SPR curve for each point for further analysis.

The impedance recording, LabView interface, parallels the SPR ones and can be performed by either commercial instrumentation (e.g., Solartron 1260 or Agilent 4294 A) or custom designed, multichannel one developed within ICB. Plane-parallel electrodes (one larger and one smaller) are custom designed in connection with the specific flow channels and SPR-sensing domains.

For dual channel evaluations (differential affinity sensing), the flow channels are 8 mm long by 0.8 mm wide with a height of 150 μm. Each flow channel is connected to an independent flow circuit controlled by a syringe pump, allowing simultaneous as well as independent analyses.

Alternatively, for whole cell analyses, a single flow cell has been designed that covers all three SPR-active regions (of the SPREETA chip).

By culturing biological cells on the conductive surface, both techniques can directly sense detailed information about cellular activities occurring on the substrate's surface allowing label-free and noninvasive study of cellular properties.

Madin–Darby Canine Kidney (MDCK) cells are frequently utilized as a model cell system surface attachment dependent. Cells attach to the surface and grow in monolayers linked together by specialized tight junctions. In culture, epithelial cells tend to experience strong contact inhibition of migration and form monolayers similar to the epithelial sheets that occur in vivo. While rather flat when cultivated in normal conditions, they round up and detach from the surface when dying.

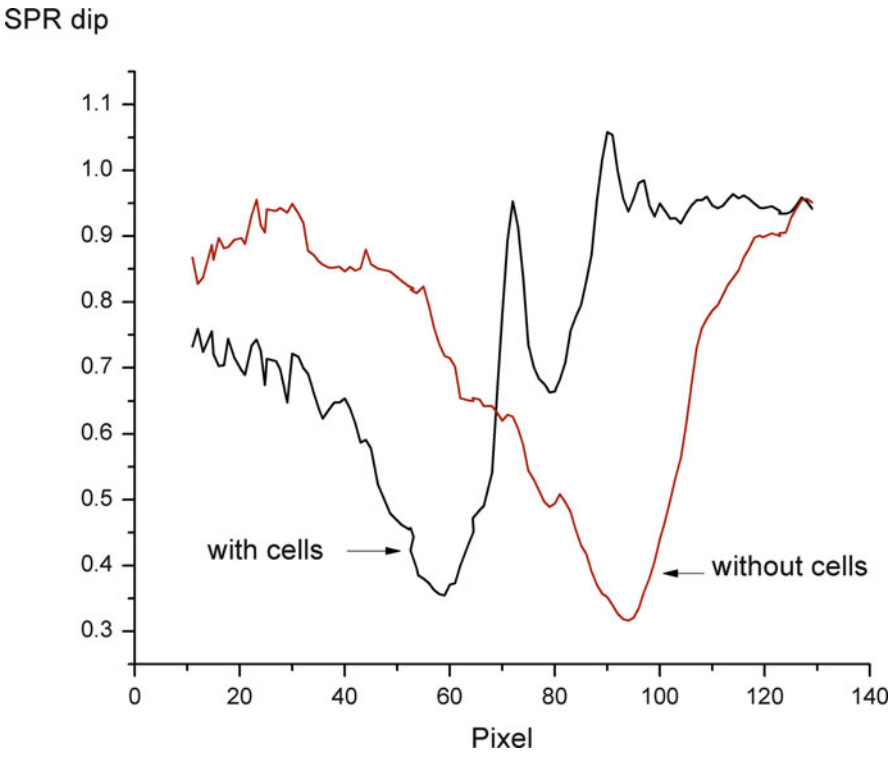

Fig. 13 SPR dip with and without MDCK cells grown on the surface

MDCK cells were grown, in controlled conditions (Dulbecco's Eagle's Medium—DMEM, Sigma supplemented with 10% Fetal Bovine Serum, 5% penicillin–streptomycin, at 37°C, 5%CO_2), to confluence on dual impedance and SPR chip, mounted in the dual measurement chamber and exposed to pore-forming compound injections.

As expected, when using the same buffer, cell presence on the sensing chip, is related to a noisier SPR curve and a shifted SPR angle as compared to cell-free chip (Fig. 13).

When cells are subjected to injections of pore-forming compounds (for generality, Triton X 100 was chosen as model analyte), the whole SPR dip structure, not only the position of the main resonance, changes, possibly indicating cell structural and morphological changes in addition to expected mass differences (when cells fully detach or the compound is adsorbed on the cellular layer).

Adequate fitting routines implemented *online* enable the derivation of the SPR angle (pixel position where reflectance minimum occurs) even on cellular platforms (with a "noisier" SPR dip).

The whole evolution, as seen in Fig. 14, during one long injection reveals highly nonmonotonous processes to be attributed to direct interaction with the cell

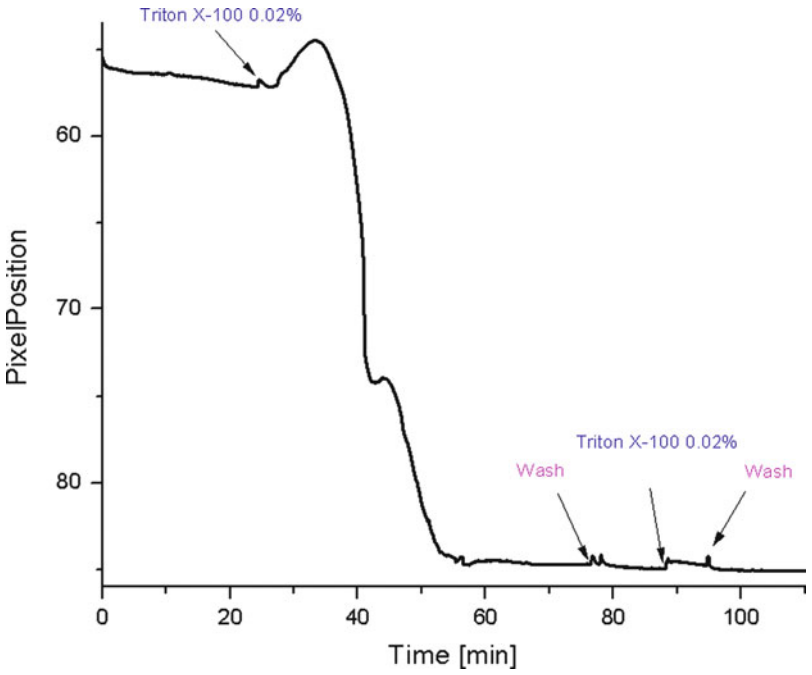

Fig. 14 Interaction between MDCK cell monolayer and a pore-forming compound as revealed by custom-made SPR set-up with integrated microfluidics

membrane, insertion, and subsequent destabilization of cell monolayer. The lack of response to a second injection proves that most of the cells were detached from the surface as confirmed by optical inspection (data not shown).

While the linear relationship between pixel position and the absolute refractive index is straightforward via calibration with standard solutions, since this calibration is rather elusive for cell platforms, in Fig. 14 the evolution of the interaction between cells and a pore-forming compound is represented via the pixel position corresponding to the derived minimum, via first derivative of the fitted SPR curve.

Quantitative ways to better characterize the richness of the SPR dip features and their particular evolutions in relation to distinct domains within the time evolution of the pixel position (this classical, "integrative" SPR information overshadows the complexity of SPR spectra in case of cells) are currently under development.

Major changes of the SPR dip were obtained in preliminary experiments on bacterial cells settling gravitationally on the surface (data not shown) proving that both bacterial and mammalian SPR platforms can be designed.

In conjunction, impedance data reveal—as seen in Fig. 15—an initial increase in Resistance and a simultaneous decrease in Capacitance values that can be related to cell swelling upon exposure to growth medium with Triton. This effect may be related to occurrence of the peak in SPR data (Fig. 14). Notably, prolonged

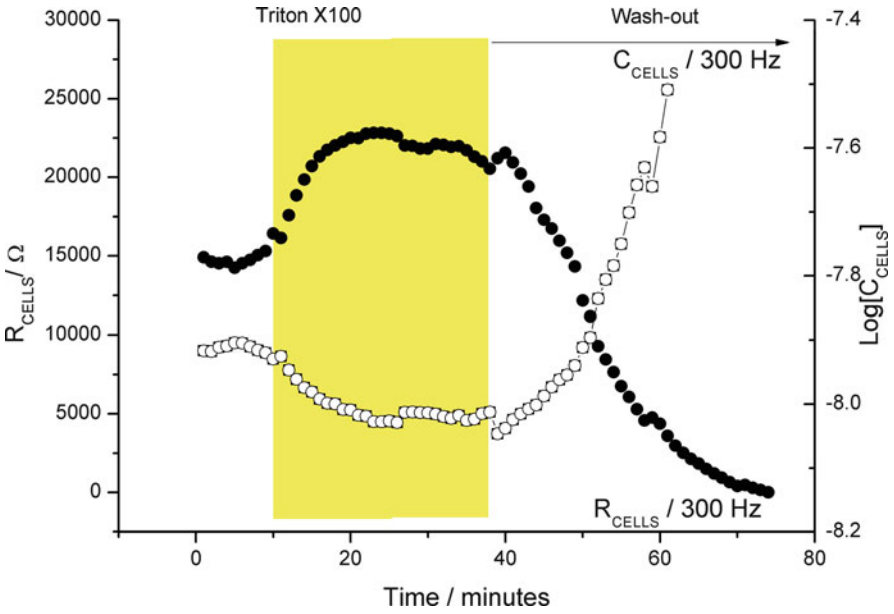

Fig. 15 Time evolution of the resistance/capacitance of the cell monolayer upon 0.02% Triton X 100 exposure

exposure to Triton X 100 destabilizes the monolayer until full detachment from the electrode layer occurs (washout region in Fig. 15).

These impedance data add to the plethora of recent reports [67–69] emphasizing the virtues of impedance spectroscopy (with or without electrochemical probes) to reveal morphological and electrical changes of cell monolayers and substantiate the effectiveness of a combined SPR-impedance cellular platform to evaluate the effect of pore-forming compounds in general and antimicrobial peptides in particular, and for detailed, real-time monitoring of the interaction process.

10 Conclusions

SPR monitoring of analyte–ligand interaction enables label-free, real-time assessment of the complex, multiphasic interaction mechanism between pore-forming compounds (including antimicrobial peptides), and model lipid matrices synthetic or cell based, paving the way for advancing SPR approaches in cell-based biosensing format.

Using specialized commercial chips (L1 Biacore) and POPC supported lipid membranes, as a first step, the entire *nonmonotonous* interaction process between melittin as a model antimicrobial peptide and zwitterionic membranes was revealed and assessed. The interaction process is quantitatively described by fitting

the experimental data with a mathematical model encompassing the distinct stages involved in peptide–lipid interaction: association, insertion of melittin into lipid matrix, pore formation, and destabilization of lipid membrane. This numerical analysis offers direct insight into representative, effective, kinetic parameters, and time evolutions of lipid and melittin concentrations during these distinct, yet interlinked phases of the entire process, and provides relevant parameters for biosensing. Consequently, the pattern of evolution of the complex, nonmonotonous process of peptide–lipid interaction and a direct way to quantify the concentration of peptide can be derived while gaining insight on interaction mechanisms depending both on various antimicrobial peptides and lipid composition of lipid membrane.

Two approaches for sensing antimicrobial peptides concentration via related effects on lipid matrix are advanced: (a) a "calibration curve" relating peptide concentration to the inverse of the characteristic peak time: $1/T_{max}$; the detection limit, e.g., in the μM range, for melittin, is imposed by the characteristic peptide: lipid thresholds dominating the complete interaction process and realistic injection times <3,600 s; (b) another one based on the threshold values and the corresponding time points of their occurrence provided by the quantitative analysis.

In an attempt to close the gap between experiments with synthetic membranes and the ones with living cells, a combined SPR-Electrical Impedance set-up is proposed. Complementary data on detergent—cell monolayer interaction as revealed by SPR and complex impedance emphasize the virtues of this combined approach for monitoring cell-pore-forming compound interaction including cell dissociation from the surface.

It is envisaged that this approach is able to support a comprehensive analysis platform, which could be further extended to a wider class of lipid matrices including mammalian and bacterial cells in relation to other pore-forming compounds, as well.

The proposed kinetic model combined with appropriate design of the experimental protocol adds a new depth to the classic SPR investigation of peptide–lipid interaction offering a quantitative platform for understanding the manifold facets of the interaction and for supporting the controlled design of new, improved antimicrobial peptides.

Acknowledgments Financial help from the Romanian National Authority for Scientific Research (program PNCDII, contract no. 81-028, 71-073, 41-013, 25 EU and 12-121) is acknowledged.

References

1. Anderluh G et al (2003) Pore formation by equinatoxin II, a eukaryotic protein toxin, occurs by induction of nonlamellar lipid structures. J Biol Chem 278(46):45216–45223
2. Chah S, Zare RN (2008) Surface plasmon resonance study of vesicle rupture by virus-mimetic attack. Phys Chem Chem Phys 10(22):3203–3208

3. Shai Y (1999) Mechanism of the binding, insertion and destabilization of phospholipid bilayer membranes by alpha-helical antimicrobial and cell non-selective membrane-lytic peptides. Biochim Biophys Acta 1462(1–2):55–70
4. Kass RS (2005) The channelopathies: novel insights into molecular and genetic mechanisms of human disease. J Clin Invest 115(8):1986–1989
5. Panchal RG et al (2002) Pore-forming proteins and their application in biotechnology. Curr Pharm Biotechnol 3(2):99–115
6. Zasloff M (2002) Antimicrobial peptides of multicellular organisms. Nature 415(6870): 389–395
7. Gheorghiu M et al (2009) Sensing based on assessment of non-monotonous effect determined by target analyte: case study on pore-forming compounds. Biosens Bioelectron 24(12): 3517–3523
8. Olaru A et al (2009) Assessment of the multiphase interaction between a membrane disrupting peptide and a lipid membrane. J Phys Chem B 113(43):14369–14380
9. Asthana N, Yadav SP, Ghosh JK (2004) Dissection of antibacterial and toxic activity of melittin: a leucine zipper motif plays a crucial role in determining its hemolytic activity but not antibacterial activity. J Biol Chem 279(53):55042–55050
10. Wessman P et al (2008) Melittin-lipid bilayer interactions and the role of cholesterol. Biophys J 95(9):4324–4336
11. Naumann R et al (1999) The peptide-tethered lipid membrane as a biomimetic system to incorporate cytochrome c oxidase in a functionally active form. Biosens Bioelectron 14(7): 651–662
12. Kim K et al (2004) Surface plasmon resonance studies of the direct interaction between a drug/intestinal brush border membrane. Pharm Res 21(7):1233–1239
13. Erb EM et al (2000) Characterization of the surfaces generated by liposome binding to the modified dextran matrix of a surface plasmon resonance sensor chip. Anal Biochem 280 (1):29–35
14. Saenko E et al (2001) Comparison of the properties of phospholipid surfaces formed on HPA and L1 biosensor chips for the binding of the coagulation factor VIII. J Chromatogr A 921(1): 49–56
15. Cha T, Guo A, Zhu XY (2006) Formation of supported phospholipid bilayers on molecular surfaces: role of surface charge density and electrostatic interaction. Biophys J 90(4): 1270–1274
16. Anderluh G et al (2005) Properties of nonfused liposomes immobilized on an L1 Biacore chip and their permeabilization by a eukaryotic pore-forming toxin. Anal Biochem 344(1):43–52
17. Habermann E, Jentsch J (1967) Sequence analysis of melittin from tryptic and peptic degradation products. Hoppe Seylers Z Physiol Chem 348(1):37–50
18. Dempsey CE (1990) The actions of melittin on membranes. Biochim Biophys Acta 1031(143–161)
19. Lundquist A et al (2008) Melittin-lipid interaction: a comparative study using liposomes, micelles and bilayer disks. Biochim Biophys Acta 1778(10):2210–2216
20. Popplewell JF et al (2007) Quantifying the effects of melittin on liposomes. Biochim Biophys Acta 1768(1):13–20
21. Frey S, Tamm LK (1991) Orientation of melittin in phospholipid bilayers. A polarized attenuated total reflection infrared study. Biophys J 60(4):922–930
22. Matsuzaki K, Yoneyama S, Miyajima K (1997) Pore formation and translocation of melittin. Biophys J 73(2):831–838
23. Lee MT et al (2008) Mechanism and kinetics of pore formation in membranes by water-soluble amphipathic peptides. Proc Natl Acad Sci USA 105(13):5087–5092
24. Zhu WL et al (2007) Cell selectivity of an antimicrobial peptide melittin diastereomer with D-amino acid in the leucine zipper sequence. J Biochem Mol Biol 40(6):1090–1094
25. Mozsolits H et al (2001) Analysis of antimicrobial peptide interactions with hybrid bilayer membrane systems using surface plasmon resonance. Biochim Biophys Acta 1512(1):64–76

26. Papo N, Shai Y (2003) Exploring peptide membrane interaction using surface plasmon resonance: differentiation between pore formation versus membrane disruption by lytic peptides. Biochemistry 42(2):458–466
27. Popplewell J et al (2005) Quantification of the effects of melittin on liposome structure. Biochem Soc Trans 33(Pt 5):931–933
28. Lee TH, Mozsolits H, Aguilar MI (2001) Measurement of the affinity of melittin for zwitterionic and anionic membranes using immobilized lipid biosensors. J Pept Res 58(6):464–476
29. Mozsolits H, Thomas WG, Aguilar MI (2003) Surface plasmon resonance spectroscopy in the study of membrane-mediated cell signalling. J Pept Sci 9(2):77–89
30. Berneche S, Nina M, Roux B (1998) Molecular dynamics simulation of melittin in a dimyristoylphosphatidylcholine bilayer membrane. Biophys J 75(4):1603–1618
31. Lin JH, Baumgaertner A (2000) Stability of a melittin pore in a lipid bilayer: a molecular dynamics study. Biophys J 78(4):1714–1724
32. Puu G (2001) An approach for analysis of protein toxins based on thin films of lipid mixtures in an optical biosensor. Anal Chem 73(1):72–79
33. Chenal A et al (2002) Membrane protein insertion regulated by bringing electrostatic and hydrophobic interactions into play. A case study with the translocation domain of diphtheria toxin. J Biol Chem 277(45):43425–43432
34. Hong Q et al (2002) Two-step membrane binding by Equinatoxin II, a pore-forming toxin from the sea anemone, involves an exposed aromatic cluster and a flexible helix. J Biol Chem 277(44):41916–41924
35. Thomas CJ, Surolia A (1999) Kinetics of the interaction of endotoxin with polymyxin B and its analogs: a surface plasmon resonance analysis. FEBS Lett 445(2–3):420–424
36. Thomas CJ, Surolia N, Surolia A (1999) Surface plasmon resonance studies resolve the enigmatic endotoxin neutralizing activity of polymyxin *B*. J Biol Chem 274 (42):29624–29627
37. Maulet Y, Brodbeck U, Fulpius B (1984) Selective solubilization by melittin of glycophorin A and acetylcholinesterase from human erythrocyte ghosts. Biochim Biophys Acta 778(3): 594–601
38. Pott T, Dufourc EJ (1995) Action of melittin on the DPPC-cholesterol liquid-ordered phase: a solid state 2H-and 31P-NMR study. Biophys J 68(3):965–977
39. Pott T, Paternostre M, Dufourc EJ (1998) A comparative study of the action of melittin on sphingomyelin and phosphatidylcholine bilayers. Eur Biophys J 27(3):237–245
40. Yu L et al (2009) Interaction of an artificial antimicrobial peptide with lipid membranes. Biochim Biophys Acta 1788(2):333–344
41. Mashaghi A et al (2008) Optical anisotropy of supported lipid structures probed by waveguide spectroscopy and its application to study of supported lipid bilayer formation kinetics. Anal Chem 80(10):3666–3676
42. Andra J et al (2008) Surface acoustic wave biosensor as a tool to study the interaction of antimicrobial peptides with phospholipid and lipopolysaccharide model membranes. Langmuir 24(16):9148–9153
43. Terry CJ et al (2006) Characterisation of membrane mimetics on a dual polarisation interferometer. Biosens Bioelectron 22(5):627–632
44. Abdiche YN, Myszka DG (2004) Probing the mechanism of drug/lipid membrane interactions using Biacore. Anal Biochem 328(2):233–243
45. Born M, Wolf E (1980) Principles of optics: electromagnetic theory of propagation, interference and diffraction of light, 6th edn. Pergamon, Oxford, p 808
46. Reitz JR, Milford FJ, Christy RW (1993) Foundations of electromagnetic theory, 4th edn. Addison-Wesley, Boston, MA, USA, p 630p
47. Peterlinz KA, Georgiadis R (1996) In situ kinetics of self-assembly by surface plasmon resonance spectroscopy. Langmuir 12(20):4731–4740
48. Schasfoort BMR, Tudos JA (eds) (2008) Handbook of surface plasmon resonance. RSC Publishing, Cambridge, UK

49. Morigaki K, Tawa K (2006) Vesicle fusion studied by surface plasmon resonance and surface plasmon fluorescence spectroscopy. Biophys J 91(4):1380–1387
50. Yang L et al (2000) Crystallization of antimicrobial pores in membranes: magainin and protegrin. Biophys J 79(4):2002–2009
51. Baird CL, Courtenay ES, Myszka DG (2002) Surface plasmon resonance characterization of drug/liposome interactions. Anal Biochem 310(1):93–99
52. Nakajima H et al (2001) Kinetic analysis of binding between Shiga toxin and receptor glycolipid Gb3Cer by surface plasmon resonance. J Biol Chem 276(46):42915–42922
53. Tamba Y, Yamazaki M (2009) Magainin 2-induced pore formation in the lipid membranes depends on its concentration in the membrane interface. J Phys Chem B 113(14):4846–4852
54. Grage SL, Afonin S, Ulrich AS (2010) Dynamic transitions of membrane-active peptides. Methods Mol Biol 618:183–207
55. Oren Z, Shai Y (1998) Mode of action of linear amphipathic alpha-helical antimicrobial peptides. Biopolymers 47(6):451–463
56. Chen X et al (2007) Real-time structural investigation of a lipid bilayer during its interaction with melittin using sum frequency generation vibrational spectroscopy. Biophys J 93(3): 866–875
57. Leontiadou H, Mark AE, Marrink SJ (2006) Antimicrobial peptides in action. J Am Chem Soc 128(37):12156–12161
58. Marrink SJ, de Vries AH, Tieleman DP (2009) Lipids on the move: simulations of membrane pores, domains, stalks and curves. Biochim Biophys Acta 1788(1):149–168
59. Ritov VB et al (1993) Alamethicin as a permeabilizing agent for measurements of Ca(2+)-dependent ATPase activity in proteoliposomes, sealed membrane vesicles, and whole cells. Biochim Biophys Acta 1148(2):257–262
60. Allende D, Simon SA, McIntosh TJ (2005) Melittin-induced bilayer leakage depends on lipid material properties: evidence for toroidal pores. Biophys J 88(3):1828–1837
61. Giaever I, Keese CR (1993) A morphological biosensor for mammalian cells. Nature 366(6455): 591–592
62. Sandu T, Vrinceanu D, Gheorghiu E (2010) Linear dielectric response of clustered living cells. Phys Rev E Stat Nonlin Soft Matter Phys 81(2 Pt 1):021913
63. Gheorghiu E, Balut C, Gheorghiu M (2002) Dielectric behaviour of gap junction connected cells: a microscopic approach. Phys Med Biol 47(2):341–348
64. Gheorghiu E (1999) On the limits of ellipsoidal models when analyzing dielectric behavior of living cells. Emphasis on red blood cells. Ann N Y Acad Sci 873:262–268
65. Gheorghiu M, Gersing E, Gheorghiu E (1999) Quantitative analysis of impedance spectra of organs during ischemia. Ann N Y Acad Sci 873:65–71
66. Ursu GA et al (2007) Sensing the cell-substrate interaction towards development of “smart” surfaces. IFMBE Proc 17(Part 4):86–89
67. Tun TN, Jenkins ATA (2010) An electrochemical impedance study of the effect of pathogenic bacterial toxins on tethered bilayer lipid membrane. Electrochem Commun 12(10):1411–1415
68. Wilkop T, Xu DK, Cheng Q (2008) Electrochemical characterization of pore formation by bacterial protein toxins on hybrid supported membranes. Langmuir 24(10):5615–5621
69. Yu NC et al (2006) Real-time monitoring of morphological changes in living cells by electronic cell sensor arrays: an approach to study G protein-coupled receptors. Anal Chem 78(1):35–43